JGR Biogeosciences

RESEARCH ARTICLE
10.1029/2019JG005205

Special Section:
Water-Energy-Carbon Fluxes Over Terrestrial Water Surfaces

The Magnitude and Drivers of Methane Ebullition and Diffusion Vary on a Longitudinal Gradient in a Small Freshwater Reservoir

R. P. McClure[1], M. E. Lofton[1], S. Chen[2], K. M. Krueger[3], J. C. Little[4], and C. C. Carey[1]

[1]Department of Biological Sciences, Virginia Polytechnic Institute and State University, Blacksburg, VA, USA, [2]UNSW Water Research Laboratory, UNSW Sydney, Sydney, New South Wales, Australia, [3]Department of Geosciences, Virginia Polytechnic Institute and State University, Blacksburg, VA, USA, [4]Department of Civil and Environmental Engineering, Virginia Polytechnic Institute and State University, Blacksburg, VA, USA

Key Points:
- CH_4 ebullition rates decreased by 98% and CH_4 diffusion decreased by 32% on a longitudinal gradient from reservoir inflow to dam
- Ebullition was driven by physical variables upstream and phytoplankton downstream; diffusion was most related to phytoplankton
- Despite large variation in CH_4 emissions longitudinally, time series models well captured the dynamics of emissions from a small reservoir

Supporting Information:
- Supporting Information S1

Correspondence to:
R. P. McClure,
ryan333@vt.edu

Citation:
McClure, R. P., Lofton, M. E., Chen, S., Krueger, K. M., Little, J. C., & Carey, C. C. (2020). The magnitude and drivers of methane ebullition and diffusion vary on a longitudinal gradient in a small freshwater reservoir. *Journal of Geophysical Research: Biogeosciences*, *125*, e2019JG005205. https://doi.org/10.1029/2019JG005205

Received 15 APR 2019
Accepted 20 FEB 2020
Accepted article online 21 FEB 2020

Abstract Reservoirs emit large amounts of methane (CH_4) to the atmosphere relative to their small surface area globally. Among the different pathways of reservoir CH_4 emissions, bubbling from the sediments (ebullition) and diffusion from the water surface are major contributors of CH_4 efflux. The magnitude of ebullition and diffusion can vary substantially over space and time in large reservoirs. However, it is unclear how the drivers of ebullition and diffusion vary along a reservoir's longitudinal gradient, particularly in small reservoirs. We measured ebullition, diffusion, and eight environmental driver variables at four transects along a longitudinal gradient within a small, eutrophic reservoir. We used time series modeling to examine how the drivers of ebullition and diffusion varied among transects. Sediment-water interface temperature, inflow discharge, and wind speed were the most important drivers of CH_4 ebullition in upstream transects of the reservoir, while phytoplankton biomass was the most important driver of ebullition in the downstream transect closest to the dam. Strikingly, CH_4 ebullition dynamics were extremely well captured by the time series models, as the modeled rates for the furthest upstream transect closely matched the observed rates throughout the monitoring period. In contrast, CH_4 diffusion dynamics were harder to model, with phytoplankton biomass as the primary driver of diffusion across all transects. Our results indicate that multiple drivers affect CH_4 emissions along a small reservoir's longitudinal gradient and should be considered when upscaling site measurements to reservoir-wide CH_4 emissions and ultimately regional or global estimates.

Plain Language Summary Freshwater reservoirs release large quantities of methane into the atmosphere. However, accurately estimating total methane release from a reservoir is challenging because the upstream area of a reservoir functions differently than the downstream area closer to the dam, likely resulting in different methane emission rates along this gradient. We measured two pathways of methane emissions, bubbling from the sediments and diffusion from the water surface, for 6 months at multiple sites in a reservoir. We also measured potential drivers of methane emissions at each site and used statistical modeling to determine how the importance of the drivers varied across different areas in the reservoir. Methane bubbling from the sediments was best predicted by physical factors such as water temperature, inflow, and wind speed in upstream sites and by phytoplankton biomass in downstream sites. Diffusion was overall best predicted by phytoplankton biomass across all sites. Our work highlights how the drivers of methane emissions can vary along the upstream-downstream gradient of a small reservoir, which can improve our understanding of how much methane is released from these ecosystems globally.

1. Introduction

Freshwater reservoirs disproportionately emit large quantities of greenhouse gases, especially methane (CH_4), to the atmosphere relative to their small surface area globally (Deemer et al., 2016). Because CH_4 has 34× the global warming potential of carbon dioxide (CO_2) over a 100-year time horizon (Myhre et al., 2013), there is growing interest in determining the magnitude and drivers of reservoir CH_4 emissions (Gunkel, 2009; Saunois et al., 2016). As reservoir construction increases globally (Zarfl et al., 2014), improving our understanding of the drivers of variability in CH_4 emissions from freshwater reservoirs is crucial for resolving global carbon emission estimates.

There are three primary pathways by which CH_4 is emitted to the atmosphere from reservoirs: bubbles released from the sediments (also known as ebullition), diffusion of dissolved CH_4 in the water through the air-water interface, and emergent plant-mediated transport through aerenchyma pores from the sediments (Bastviken et al., 2004). In the absence of emergent plants, the dominant processes are ebullition and diffusion. Ebullition rates depend on the production and release of CH_4 bubbles from the sediments, and diffusion rates depend on the difference in the CH_4 concentration between the water and the atmosphere and the physical rate of gas exchange (Bastviken et al., 2004). The relative proportion of diffusion versus ebullition can vary widely in reservoirs, ranging from a CH_{4diff}:CH_{4ebu} ratio of 0.01 to 18 (Deemer et al., 2016), and thus, quantifying both pathways is needed to estimate total reservoir CH_4 emissions.

Within reservoirs, CH_4 ebullition and diffusion rates can vary substantially along a longitudinal gradient from the upstream areas near the major inflows to the downstream areas near the dam (Beaulieu et al., 2014, 2016; Huang et al., 2017; Sobek et al., 2012; Tušer et al., 2017). Ebullition is generally highest in shallow areas upstream, with much lower (but still detectable) rates in downstream areas (Beaulieu et al., 2016, 2018). Similarly, studies have also demonstrated that the highest diffusion rates occur in shallow upstream sites and decrease toward the deeper sites in larger reservoirs (Beaulieu et al., 2016; Yang et al., 2013). This longitudinal heterogeneity has been well documented in large reservoirs (surface area > 0.5 km^2; DelSontro et al., 2010; Demarty et al., 2011; Marcelino et al., 2015; Soumis et al., 2004; Tušer et al., 2017), but it remains unknown how variable CH_4 emissions are on a longitudinal gradient within small reservoirs (surface area < 0.5 km^2), which may exhibit less predictable reservoir zonation because of their size.

In addition to their spatial variation, ebullition and diffusion rates can also vary temporally. In temperate reservoirs, ebullition is generally low in the early spring and increases from midsummer into early autumn and then decreases before fall turnover (Martinez & Anderson, 2013; Tušer et al., 2017). Likewise, elevated diffusion rates in reservoirs have been observed in early spring after ice-off and then decrease or remain stable into the summer and early autumn (Huttunen et al., 2002). At or shortly before fall turnover, diffusion rates in both naturally formed lakes and reservoirs reach their annual peak as dissolved CH_4 that accumulates in the hypolimnion during the thermally stratified summer period is mixed into the epilimnion and brought to the surface (Bastviken et al., 2004; Huttunen et al., 2002).

Studies of CH_4 emissions in naturally formed lakes and reservoirs have suggested that ebullition and diffusion rates are controlled by both physical and biological variables (West et al., 2016), with the relative importance of these drivers likely varying spatially (Beaulieu et al., 2016; DelSontro et al., 2016; Hofmann, 2013; Natchimuthu et al., 2016; Tušer et al., 2017; Yang et al., 2013). For example, CH_4 ebullition rates have been shown to be related to shear stress at the sediment-water interface (SWI) caused by bottom currents (Joyce & Jewell, 2003; Yang et al., 2013), elevated wind speeds (Joyce & Jewell, 2003), changes in barometric pressure (Casper et al., 2000; Mattson & Likens, 1990; Peltola et al., 2018; Tokida et al., 2005; Yu et al., 2014), and varying depth (Tušer et al., 2017), all factors that may vary along a longitudinal gradient in a reservoir. Similarly, increases in temperature at the SWI during the summer, particularly in shallower sites, increase ebullition rates (Aben et al., 2017; DelSontro et al., 2016). In addition to these physical drivers, recent meta-analyses show strong positive associations between primary productivity and ebullition (Deemer et al., 2016; DelSontro et al., 2016; DelSontro et al., 2018). Prior studies conducted at the microcosm to whole-ecosystem scale have revealed that increased chlorophyll *a* concentrations increase ebullition rates by providing labile substrate available for methanogenesis from autochthonous production (Schwarz et al., 2008; West et al., 2012, 2016; Zhou et al., 2019).

Similar to ebullition, diffusion rates are also influenced by multiple factors that can vary spatially (Beaulieu et al., 2016). For example, increasing near-surface turbulence and increasing winds can increase the magnitude of CH_4 diffusing across the air-water interface (Bastviken et al., 2004; Poindexter et al., 2016; Poindexter & Variano, 2013; Yang et al., 2013). In addition, elevated epilimnetic autochthonous production can increase CH_4 diffusion by providing labile organic matter to the sediments, which can stimulate pore water methanogenesis (Peeters et al., 2019), as well as providing labile material for oxic CH_4 production and generating anoxic microniches that produce CH_4 in the water column (Bižić et al., 2020; Bogard et al., 2014).

Quantifying ecosystem-scale CH_4 emission rates in combination with their drivers is difficult because of spatial heterogeneity in environmental variables, which necessitates extensive spatial sampling to avoid biased

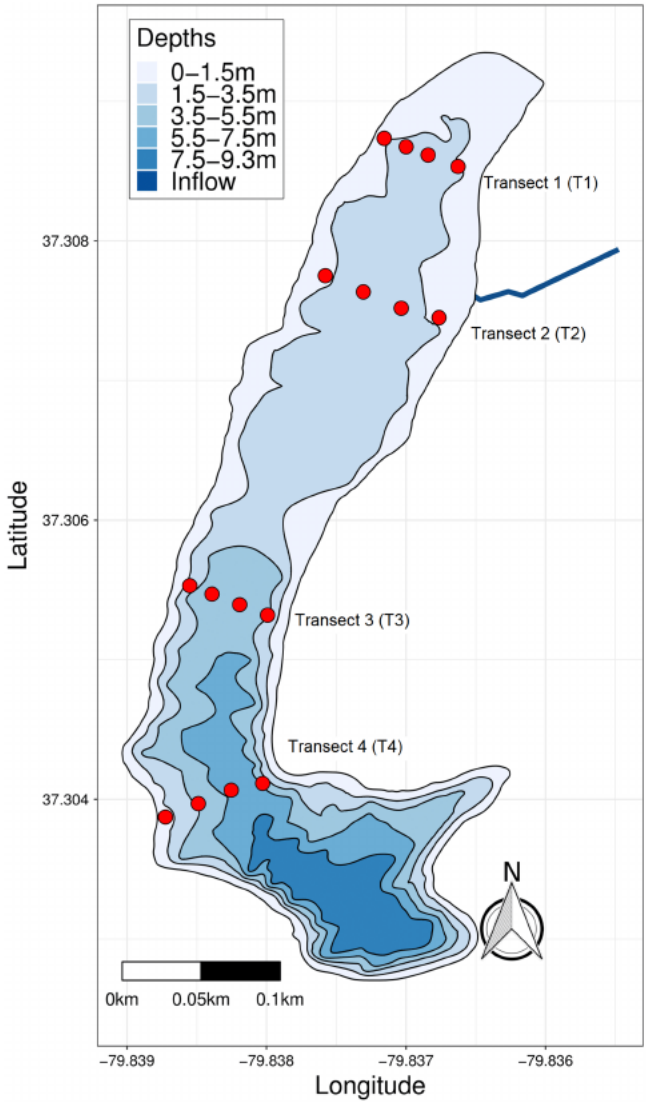

Figure 1. Falling Creek Reservoir's bathymetric map. We deployed 16 ebullition traps denoted by the red dots along the longitudinal gradient for the 2017 monitoring period. CH_4 diffusion was measured at each ebullition site during the same period. Four traps were deployed on four transects (T1–T4) that extended along the open-water fetch axis of Falling Creek Reservoir's longitudinal gradient.

estimates (Beaulieu et al., 2016; Wik et al., 2016). Previous studies that have estimated spatial variation in the drivers of CH_4 emissions in reservoirs have primarily been conducted in larger reservoirs (Deemer et al., 2016). While these past studies have consistently documented longitudinal variability in the magnitude of CH_4 emissions (DelSontro et al., 2010; Demarty et al., 2011; Marcelino et al., 2015), there remains a limited understanding of how the *drivers* of CH_4 emissions may also vary longitudinally, as well as whether these spatial differences exist in small reservoirs.

To address this gap, we simultaneously measured ebullition and diffusion and potential environmental predictors at multiple sites along a longitudinal gradient in a small temperate reservoir throughout an ice-free period. We used time series modeling to examine if the drivers of both CH_4 emission rates varied among sites during the monitoring period. Our goal was to improve our understanding of how the rates of CH_4 ebullition and diffusion vary spatiotemporally and how different environmental variables interact to regulate the magnitude of CH_4 ebullition and diffusion emissions in small reservoirs (<0.5 km^2), which encompass 88% of the ~87,000 monitored reservoirs in the conterminous United States (National inventory of dams, 2018).

2. Materials and Methods

2.1. Site Description

We studied CH_4 emission rates and their drivers in Falling Creek Reservoir (FCR), a eutrophic drinking water reservoir located in southwest Virginia, USA (37.30°N, 79.84°W). FCR is a small (surface area = 0.119 km^2) and shallow (Z_{max} = 9.3 m, Z_{mean} = 4.0 m) reservoir with one primary inflow stream from an upstream reservoir (Figure 1). FCR is dimictic and thermally stratified between late April and mid-October (Gerling et al., 2016; McClure et al., 2018). The reservoir was constructed in 1898 and is owned and managed by the Western Virginia Water Authority. The Western Virginia Water Authority managers maintain the reservoir at a constant depth of 9.3 m throughout the year. FCR has limited emergent plant abundance, motivating our focus on ebullition and diffusion as the primary CH_4 pathways from the reservoir.

2.2. CH_4 Emissions

2.2.1. CH_4 Ebullition

We sampled ebullition rates in FCR weekly from 15 May to 23 October 2017 using ebullition traps (Keller & Stallard, 1994). Four transect lines were deployed in the reservoir to capture the longitudinal gradient of FCR. Each transect line had four evenly spaced inverted funnel traps (n = 16 traps total; Figures 1, S1, and S2 in the supporting information). Transects T1 and T2 represented shallower areas of FCR and captured conditions typical of upstream reservoir sites near inflow tributaries with warmer SWI temperatures (Figure 1). Transects T3 and T4 were deeper than T1 and T2 and exhibited characteristics typical of downstream areas of reservoirs that are more lacustrine in nature (Figure 1). The T4 transect was placed at the deepest site of FCR that was still located on the same fetch axis as the other transects to capture any organic matter deposition from upstream (Figure 1).

Each 0.26-m^2 ebullition trap was placed 0.5 m below the water surface to capture CH_4 bubbles that were released from the sediments underneath the trap (Figures S1 and S2). A sealed tube extended from the bottom of the funnel to 0.1 m above the water surface through a foam float that kept the trap in place. The top of the inverted funnel's tubing was fitted with a 25-mm plastic threaded ball valve that was sealed with a rubber septum stopper (Suba-Seal Septa, MilliporeSigma, St. Louis, MO, USA). The valve and the septum prevented

ebullition gas from escaping out of the top of the funnel (Figure S2). When the traps were first deployed, reservoir water was siphoned to the top of the traps using a syringe and needle through the septa. When rising CH_4 bubbles were caught in the funnel trap, the siphoned water at the top of the tube was displaced with gas, which stayed in the top of the tube until the gas was sampled weekly.

We collected ebullition gas from every trap each week during the monitoring period. Before sampling, the small space between the ball valve and the septum stopper was preevacuated, ensuring that only gas that entered the funnel from the reservoir was collected in the trap. After the space was evacuated, the ball valve was opened, and ebullition samples were extracted across the septum stopper using a needle attached to a 10-ml syringe. Up to 10 ml of gas was injected into a 12-ml crimp top glass vial that was prefilled with salt brine solution. A secondary exit syringe extracted the salt brine solution as the sample was injected to generate 10 ml of gas headspace in the vial. If enough gas sample was available, two replicates were collected from each trap. The vials were stored upside down until analysis, so the remaining 2 ml of salt brine solution acted as a barrier to prevent any gas from escaping. We extracted any remaining gas in the trap using a 30-ml syringe and summed the total volume of gas collected each week.

The gas samples were analyzed using a gas chromatograph coupled with a flame ionization detector within 24 hr of collection (following McClure et al., 2018). We determined the ebullition rate as follows:

$$\textit{Daily } \mathrm{CH_4} \textit{ ebullition rate } \left(\mathrm{mg\ CH_4\ m^{-2}\ day^{-1}}\right) = \frac{V_{\mathrm{gas}}[CH_4]}{(T_{\mathrm{d}})A_{\mathrm{F}}}, \quad (1)$$

where V_{gas} is the volume of gas in the trap (L), $[CH_4]$ is the CH_4 concentration of the gas (mg CH_4 L^{-1}), T_{d} is the duration of time the trap was deployed (in days), and A_{F} is the cross-sectional area of the funnel (0.26 m^2). The calculated ebullition rate therefore represents an integration of the total gas captured per unit area during T_{d}. We calculated the daily ebullition rate separately for each trap every week and then averaged the rates from the four traps within each transect (T1–T4) to determine a mean daily transect ebullition rate for each week. We then determined the seasonal ebullition rate for each trap during the monitoring period by summing all of the weekly $V_{\mathrm{gas}}[CH_4]$ masses collected throughout the monitoring period and dividing this sum by the A_{F} and the total number of days the traps were deployed (n = 161 days in total from May to October). We averaged the seasonal ebullition rate of all the traps in a transect to calculate the mean seasonal transect ebullition rate and calculated the reservoir-wide mean seasonal ebullition rate by averaging each individual trap's seasonal ebullition rate.

2.2.2. CH_4 Diffusion

We measured CH_4 diffusion rates across the air-water interface at each of the sampling sites (Figure 1) using the floating chamber method (Gålfalk et al., 2013; Podgrajsek et al., 2014). We deployed the chamber ~1 m from each ebullition trap from a boat at the same time the ebullition traps were being sampled. The chamber was constructed using an inverted opaque bucket with a volume of 0.02 m^3 and an area of 0.15 m^2. The trap was fitted with foam so that the lip of the chamber sat ~3 cm below the water surface to seal the inside of the chamber from the surrounding air. We prevented internal heating within the chamber while it was deployed by wrapping the outside of the chamber with reflective aluminum tape. Two airtight gas ports were fitted at the top of the chamber and connected to two separate 3-m sections of 0.635-cm Tygon PVC tubing, which were in turn connected to the inlet and waste valves of a Los Gatos ultraportable greenhouse gas analyzer (UGGA; Los Gatos Research Inc., San Jose, CA, USA). The UGGA circulated air through the chamber at ~405 ml min^{-1} and recorded moisture-corrected CH_4 (ppm) on 10-s intervals.

We allowed the chamber to float freely on the water surface and collect data for at least 5 min at each site before it was vented to the atmosphere. We used a short incubation time because we were interested in instantaneous diffusion rates and did not intend to parse out ebullition from diffusion. If ebullition bubbles were observed when the chamber was deployed, we removed the chamber from the water surface, held it open to the atmosphere, and waited 1 min to allow any CH_4 from the ebullition bubble to circulate out of the chamber before placing it back onto the surface. The daily diffusion rates were calculated as follows:

$$\textit{Daily } CH_4 \textit{ diffusion rate } \left(\text{mg } CH_4\ \text{m}^{-2}\ \text{day}^{-1}\right) = \frac{s \times V_{ch}}{A_{ch}} \times 1,440\ \text{min day}^{-1}, \quad (2)$$

where s is the slope of a linear regression of the concentrations of CH_4 in the chamber plotted over time (mg $CH_4\ L^{-1}\ min^{-1}$), V_{ch} is the total volume of the chamber (including the chamber, tubing, and volume inside the UGGA in L), and A_{ch} is the area of the chamber at the opening to the water surface (0.15 m^2). We then scaled the instantaneous diffusion rate for each site to a daily rate by multiplying the instantaneous diffusion (in units of mg $CH_4\ m^{-2}\ min^{-1}$) by 1,440 min day^{-1} (the number of minutes within 1 day). We averaged the rates (in units of mg $CH_4\ m^{-2}\ day^{-1}$) from the four sites within each transect (T1–T4) to determine the mean daily transect diffusion rate for each week.

To compare the diffusion rates with the mean seasonal ebullition rates for each transect, which integrated week-long ebullition collection, we scaled the daily diffusion rates from each site to the week by multiplying by the number of days between measurements. We then summed the weekly diffusion from each site throughout the monitoring period (in mg $CH_4\ m^2$) and then divided by the total number of days sampled ($n = 161$) to calculate the seasonal rate. We averaged seasonal diffusion rates from the four sites within a transect to calculate the mean seasonal transect diffusion rate. Finally, to compare the reservoir-wide diffusion rates to ebullition rates, we averaged all seasonal site rates (in units of mg $CH_4\ m^{-2}\ day^{-1}$) over the monitoring period to calculate the reservoir-wide mean seasonal diffusion rate. Fluxes from all 16 sites were measured during the daytime period between 10:00 and 16:00 throughout the May-October monitoring period. It is important to note that diffusion rates were possibly underestimated because of the assumption that diffusive rates between 10:00 and 16:00 were representative of the total diel period, which excludes the higher diffusion rates that can occur outside this time due to convective mixing (Anthony & MacIntyre, 2016). The CH_4 ebullition and diffusion data sets are available through the Environmental Data Initiative repository (McClure et al., 2019).

2.3. CH_4 Emission Predictors

We selected candidate driver variables by identifying previously published predictors of CH_4 ebullition and diffusion at the ecosystem scale that could feasibly be sampled at FCR. The variables included depth (Deshmukh et al., 2014; Tušer et al., 2017), inflow discharge (Maeck et al., 2014), SWI temperature (Aben et al., 2017), phytoplankton biomass (West et al., 2016), change in atmospheric pressure (Tokida et al., 2007; Zhu et al., 2016), wind speed (Joyce & Jewell, 2003), and near-sediment and surface water turbulence (Joyce & Jewell, 2003; Yang et al., 2013). Dissolved oxygen at the SWI at each transect was measured but not included in the analysis because of sensor failure during the monitoring period.

2.3.1. Mean Transect Depth

We determined the depth of each transect using a Portable Water Depth Sounder Gauge (Cole-Parmer, Vernon Hills, IL, USA). We first determined the depth of all the traps along FCR's longitudinal gradient ($n = 16$ traps; Figure 1). We then determined the mean depth of each transect by adding up the total depth (m) of the traps in each transect and then divided by the number of traps ($n = 4$ traps) across the transect (McClure et al., 2019).

2.3.2. Inflow Discharge

We determined the inflow discharge into FCR using a weir ~150 m upstream from the major stream outlet into the reservoir. Discharge was determined every 15 min using an INW Aquistar PT2X pressure sensor (INW, Kirkland, WA, USA; Gerling et al., 2016; Carey, Gerling, et al., 2018; Carey, Lofton, et al., 2018). Details on the weir and pressure transducer are described by Carey, Gerling, et al. (2018) and Carey, Lofton, et al. (2018). There are no lower-order streams or known groundwater sources that enter the stream between the weir and the outlet to the reservoir (Figure 1).

2.3.3. SWI Temperatures

We collected high-resolution temperature data at each ebullition trap during the monitoring period. Two temperature loggers (HOBO Pendant Temperature/Light Data Logger, Bourne, MA, USA) was deployed at each ebullition trap during the monitoring period and recorded data on 10-min intervals. One logger was sunk using a stainless-steel weight and a nylon string to sit ~10 cm above the SWI to determine the SWI temperature. We affixed the bottom logger ~1 m horizontally away from the passive funnel traps to prevent disturbance of sediments under the traps if movement of the transect lines caused the logger to come

into contact with the sediments. The other logger was deployed on each trap, just below the water's surface (McClure et al., 2019).

We used temperature data from the surface and SWI loggers to determine the day of fall turnover in the reservoir. Because shallow upstream sites were expected to exhibit isothermal water column temperatures earlier than the deeper stratified sites, we determined fall turnover as the date that the temperature loggers at the SWI on transect T4 (Figure 1) were <1 °C different from the temperature at the water surface, following McClure et al. (2018).

2.3.4. Transect Phytoplankton Biomass

We collected high-resolution water-column depth profiles of total phytoplankton biomass at each of the transects using an in situ fluorometer. The ~15-cm-resolution profiles were taken from the center of each transect at the same time we sampled CH_4 ebullition and diffusion, using a calibrated FluoroProbe (bbe Moldaenke, Schwentinental, Germany). The Fluoroprobe is a submersible fluorometer that uses multiple wavelengths to measure concentrations of total phytoplankton biomass in units of μg phytoplankton L^{-1} (Catherine et al., 2012; Kring et al., 2014; Ouellet Jobin & Beisner, 2014). We determined the mean phytoplankton biomass at each transect by averaging the values of the water column profile (Carey, Gerling, et al., 2018; Carey, Lofton, et al., 2018).

2.3.5. Barometric Pressure and Wind Speed

Because CH_4 ebullition emissions are more closely related to changes in barometric pressure than absolute barometric pressure (Tokida et al., 2005), we calculated the first difference of week-to-week mean barometric pressure (Δ *pressure*). We first averaged all pressure values measured in between sampling days with a CS106 Standard Barometer (Campbell Scientific, Logan, UT, USA) deployed on FCR's dam as part of the meteorological station. We assumed that the minute-resolution barometric pressure data recorded at the dam station were representative of all of FCR's small surface area. We then subtracted the mean pressure measured in the prior week from the mean pressure recorded during the sampling week. Positive *pressure* values between sampling periods indicated an increase in mean pressure at the reservoir surface, and a negative change indicated a decrease in pressure from the previous week.

Wind speeds were determined with a 05103-L Wind Monitor (Campbell Scientific, Logan, UT, USA) deployed on FCR's dam as part of the same meteorological station. We calculated mean wind speed during each week of the CH_4 ebullition and diffusion sampling period using minute-resolution wind speed data (Carey et al., 2019).

2.3.6. Water Turbulence

We estimated water turbulence as turbulent kinetic energy at the near-sediment and the surface at each transect (T1–T4) using a calibrated three-dimensional hydrodynamic model (Si3D) in lieu of direct measurements. The Si3D hydrodynamic model is a semi-implicit three-dimensional computational fluid dynamics code that adopts a finite-difference method for numerically solving the Reynolds-averaged Navier-Stokes equations for momentum, transport equations for temperature, and equations that relate water temperature to density (Rueda & Schladow, 2003; Rueda & Schladow, 2009). The Si3D model provides outputs that are highly resolved over space and time and allows a user to analyze physical processes of lake circulation (Rueda & Schladow, 2003). A detailed description of the Si3D model is provided by Rueda and Schladow (2003), and the hydrodynamics in Si3D were validated following Smith (2006).

For our study, a three-dimensional numerical grid using 5 m × 5 m × 0.3 m (L × W × H) cells was generated for the entire reservoir based on the bathymetry of FCR. Driver data for Si3D include shortwave radiation (W m^{-2}), air temperature (°C), atmospheric pressure (Pa), relative humidity (%), cloud cover (%), and the zonal and meridional wind speeds (m s^{-1}), which were all measured by the meteorological station located on the dam of FCR and the discharge from FCR's primary inflow into the reservoir. The Si3D calibration for FCR was validated by Chen et al. (Chen et al., 2017; Chen et al., 2018), who reported good consistency between the field and numerical results for reservoir mixing.

We determined the near-sediment turbulence below each of the ebullition traps by running Si3D for 1-week intervals at 5-s timesteps, which generated model output of instantaneous velocity in the *x*, *y*, and *z* axes for each grid cell. First, we determined the perturbation velocity (in cm s^{-1}), which is the difference between the instantaneous velocity at each timestep and the mean velocity in all three axes in each grid cell over the

week-long time interval (Garratt, 1994). Second, we used the mean perturbation velocities to calculate near-sediment turbulence for each ebullition trap using the following equation:

$$Turbulence\ (TKE) = 0.5\sqrt{\overline{u'^2} + \overline{v'^2} + \overline{w'^2}}, \tag{3}$$

where u', v', and w' are the components of mean perturbation water velocity along the x, y, and z axes, respectively (Garratt, 1994). Third, we calculated the mean transect-level near-sediment turbulence by averaging the turbulence for all ebullition traps in each transect between weekly samplings. We repeated these calculations to calculate turbulence at the near surface, using the model output for the grid cell at the surface layer by each ebullition trap (Figure S3). The modeled near-sediment and near-surface turbulence data are available in the Environmental Data Initiative repository (McClure et al., 2019).

2.4. Statistical Analyses

We first analyzed the CH_4 ebullition and diffusion rates measured at each individual site to examine if there was more variability in CH_4 emissions within or among transects. This analysis was used to determine if small reservoirs such as FCR exhibited longitudinal variability in their CH_4 emissions. To do this, we analyzed the spatial coherence of ebullition and diffusion at each site following Carey et al. (2014). We calculated the Spearman rank correlations of ebullition rates among all sites over the May-October monitoring period and then compared these to within-transect site correlations of ebullition. A greater coherence within transects than among transects supported subsequent analyses examining the drivers of CH_4 ebullition aggregated to the transect level. We then repeated this analysis for CH_4 diffusion rates.

After it was determined that FCR exhibited longitudinal variability in CH_4 emissions, we used time series modeling to determine if the drivers of CH_4 ebullition and diffusion rates varied on the longitudinal gradient in FCR. Given that we were limited to 23 weeks of data, our goal was to identify the most important time series models predicting CH_4 ebullition and diffusion rates throughout the entire monitoring period at each transect and aggregated across the reservoir. CH_4 ebullition and diffusion rates were significantly temporally autocorrelated on a 1-week time lag (Spearman's rank correlation; $r = 0.73$ for ebullition and $r = 0.38$ for diffusion). As a result, we used a separate autoregressive (AR) time series model with an AR1 lag term to predict mean CH_4 ebullition and diffusion at each transect (Box & Pierce, 1970). Including the AR1 term in our time series models was essential for controlling for the inherent time dependence of the CH_4 emissions week to week. We analyzed the mean transect emission rates and not site-specific rates for the AR1 time series models because our focus was on the generalized differences between upstream and downstream drivers in CH_4 emissions and not site-specific drivers unique to FCR. Finally, we also averaged the CH_4 ebullition and diffusion rates across the four transects to run a reservoir-wide AR1 time series model.

Because many potential environmental predictors were collinear, we excluded variables with Spearman rank correlations that had $r > 0.5$, using univariate scatterplots to choose the best fitting predictor. We ln-transformed CH_4 ebullition, diffusion, near-sediment and surface turbulence, wind speed, inflow discharge, and phytoplankton biomass to meet the assumptions of normality. The global equation with all possible environmental predictors was

$$\begin{aligned} ln\left(CH_4 Emission_{(t)}\right) = ln\left(CH_4\, Emission_{(t-1)}\right) + \left(Phytoplankton\ \ biomass_{(t)}\right) + \\ ln\left(Sediment\ \ turbulence_{(t)}\right) + ln\left(Surface\, turbulence_{(t)}\right) + SWI\ temperature_{(t)} + \\ \Delta pressure + ln\left(Mean\ \ wind\ \ speed_{(t)}\right) + ln\left(Inflow\ discharge_{(t)}\right) + Depth + \varepsilon, \end{aligned} \tag{4}$$

where $ln(Phytoplankton\ biomass_{(t)})$ was used as a metric of phytoplankton production and $ln(Sediment\ turbulence_{(t)})$ and $ln(Surface\ turbulence_{(t)})$ were metrics of the movement of water near the sediment and water surface, respectively. $SWI\ temperature_{(t)}$ was a metric of the sediment temperature. Δ *pressure* was the first difference of mean weekly atmospheric pressure measured at the reservoir surface, and $ln(Mean\ wind\ speed_{(t)})$ represented the mean wind speed during the duration of time we sampled the CH_4 emission rates for each sampling date. $ln(Inflow\ discharge_{(t)})$ represented the mean discharge during each week ebullition and diffusion were collected. Finally, we also included *Depth* as a driver variable.

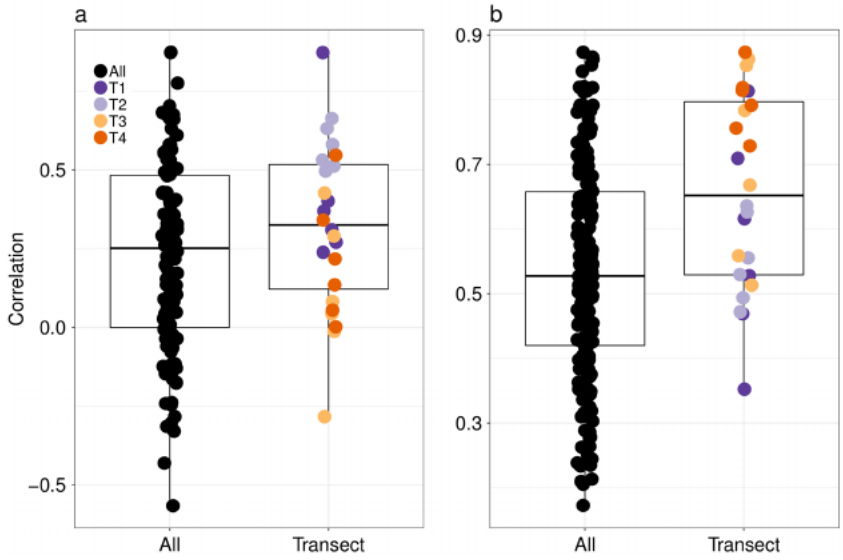

Figure 2. Box plots summarizing the pairwise spatial coherence (indicated by Spearman rank correlation) of weekly CH_4 ebullition (a) and CH_4 diffusion rates (b) at the four sites within each of the four transects in the reservoir. Coding indicates correlations among all sites within the reservoir regardless of transect (All) versus at different sites within the same transect (Transect). The colors denote the identity of the transect where the within-transect correlations were measured.

We used the corrected Akaike Information Criterion (AICc) to compare AR1 models with all selected environmental predictors at each separate transect and aggregated across all transects in FCR. We used AICc as the main metric for evaluating models and not R^2 to ensure a balance between goodness-of-fit and model parsimony (Quinn & Keough, 2002). AICc was more likely to identify a model that was not overfitting the data, thus enabling potential scaling to other ecosystems. We also compared the predicted CH_4 ebullition and diffusion rates from the highest-ranked AICc model with the observed rates at each separate transect and aggregated across all transects to assess model performance throughout the monitoring period. Finally, we compared AICc ranked AR1 models individually for all 16 sites (Table S1). However, given our research objective to quantify longitudinal patterns in CH_4 fluxes, the analysis below is focused on the transect-level and reservoir-level models. All analyses were conducted using R version 3.6.0 (R Core Team, 2018).

3. Results

3.1. Spatial Coherence of CH_4 Emissions

There was greater spatial coherence in CH_4 emissions at sites within transects than among all sites for both ebullition and diffusion in FCR (Figure 2), suggesting that FCR exhibited longitudinal variability in CH_4 emissions. Because of the coherence results, we subsequently focused on emissions aggregated by transect, rather than individual sites, to determine the most important drivers of ebullition and diffusion along the reservoir's longitudinal gradient during the monitoring period. All individual site data are available in Figure S4.

3.2. Seasonal CH_4 Emission Rates

We observed much higher CH_4 ebullition rates and slightly higher CH_4 diffusion rates at upstream transects T1 and T2 than at downstream transects T3 and T4 (Figure 3), providing further evidence of longitudinal variability in CH_4 emissions in FCR. Mean seasonal ebullition rates were highest at T1 (36 ± 12 [1 SE] mg CH_4 m^{-2} day^{-1}) and then lowered by ~50% at T2 (16 ± 9.9 mg CH_4 m^{-2} day^{-1}). Ebullition rates continued to lower at the two downstream transects, with 10 ± 6.9 mg CH_4 m^{-2} day^{-1} at T3 and 0.63 ± 0.36 mg CH_4 m^{-2} day^{-1} at T4. Mean seasonal diffusion rates were also highest at upstream transects T1 and T2 at 6.9 ±

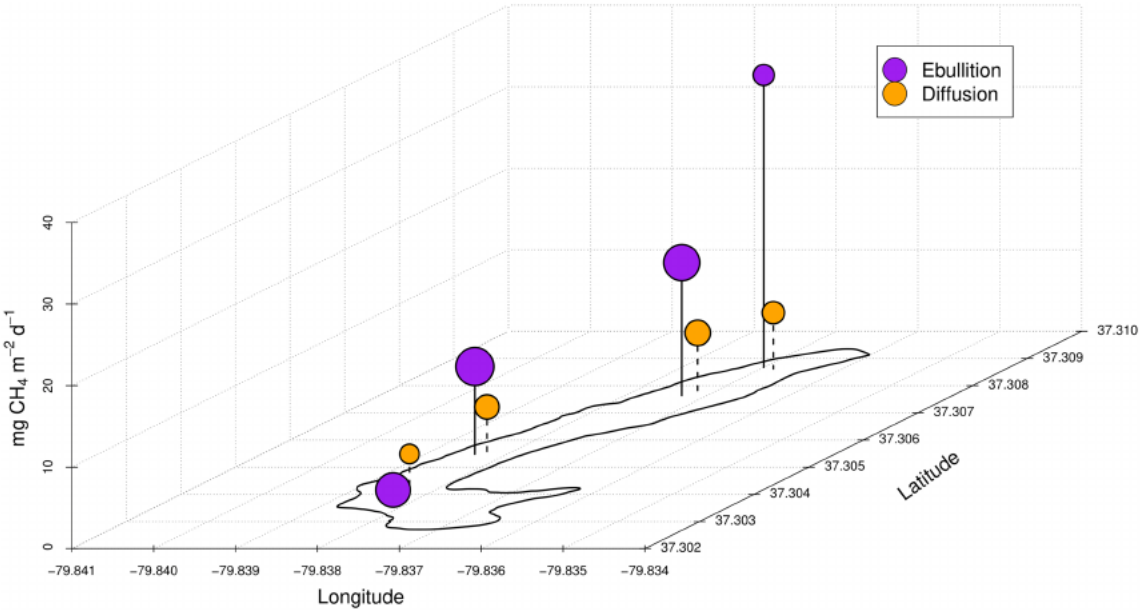

Figure 3. Mean seasonal CH_4 emission rates observed during the 2017 ice-free monitoring period. The height of the vertical solid lines represents the magnitude of the mean seasonal CH_4 ebullition rate at each transect, and the height of the vertical dashed lines represents the mean seasonal diffusion rate at each transect. The diameter of the spheres on top of each line is sized relative to the coefficient of variation of the emission rates measured at each trap on that transect (n = 768 observations; 384 each for ebullition and diffusion).

0.73 and 8.0 ± 1.1 mg CH_4 m^{-2} day^{-1}, respectively, and then decreased by 15–40% at downstream transects T3 and T4 with 6.0 ± 0.44 and 4.7 ± 0.47 mg CH_4 m^{-2} day^{-1}, respectively.

Aggregated across all transects in FCR and over the monitoring period, the mean seasonal reservoir-wide ebullition rate was 16.0 ± 7.4 mg CH_4 m^{-2} day^{-1}, and the mean seasonal reservoir-wide diffusion rate was 6.4 ± 1.2 mg CH_4 m^{-2} day^{-1}, resulting in a reservoir-wide CH_{4diff}:CH_{4ebu} ratio of 0.40 ± 0.19. transects T1 and T2 had higher ebullition rates compared to diffusion, with a combined seasonal CH_{4diff}:CH_{4ebu} ratio of 0.28 ± 0.11, while the T3 and T4 transects had higher diffusion rates than transects T1 and T2, with a combined seasonal CH_{4diff}:CH_{4ebu} ratio of 0.94 ± 0.26 (Figure S4).

3.3. Daily CH_4 Emission Rates

We observed high spatial and temporal variation in the mean transect daily ebullition rates in FCR (Figure 4a). Daily ebullition rates across all transects remained low (<6 mg CH_4 m^{-2} day^{-1}) from 15 May though 5 June (Figure 4a). In early summer, daily ebullition rates from transects T1–T3 increased until the peak maximum ebullition rate was observed at T3 on 24 July and T1 and T2 on 31 July, while T4 daily ebullition rates exhibited no substantial increase or defined peak throughout the monitoring period. Peak rates were highest at the riverine transects, reaching up to 185 mg CH_4 m^{-2} day^{-1} at T1 on 31 July. By 4 September, ebullition rates from all sites had decreased to <15 mg CH_4 m^{-2} day^{-1} and then remained below ~25 mg CH_4 m^{-2} day^{-1} for the remainder of the monitoring period.

Compared to ebullition, we observed less spatial but still high temporal variation in the mean transect daily CH_4 diffusion rates in FCR (Figure 4b). On the first date of sampling (15 May), we observed elevated diffusion rates from T1 and T2 (18 and 22 mg CH_4 m^{-2} day^{-1}, respectively) and lower diffusion rates from T3 and T4 (~10 mg CH_4 m^{-2} day^{-1}). Diffusion remained low (<10 mg CH_4 m^{-2} day^{-1}) until mid-July and then exhibited a small increase between 24 July and 1 October but never reached higher than 20 mg CH_4 m^{-2} day^{-1} at each site. Starting 1 October, the daily diffusion rates from all transects increased (rates of increase were 1.1 mg CH_4 m^{-2} day^{-1} for T1, 1.7 mg CH_4 m^{-2} day^{-1} for T2, 0.9 mg CH_4 m^{-2} day^{-1} for T3, and 0.6 mg CH_4 m^{-2} day^{-1} for T4), and all transects reached their highest observed diffusion rate of the season on 16 October, which closely coincided with fall turnover on 17 October (see below). Diffusion rates after turnover decreased back to levels similar to spring observations.

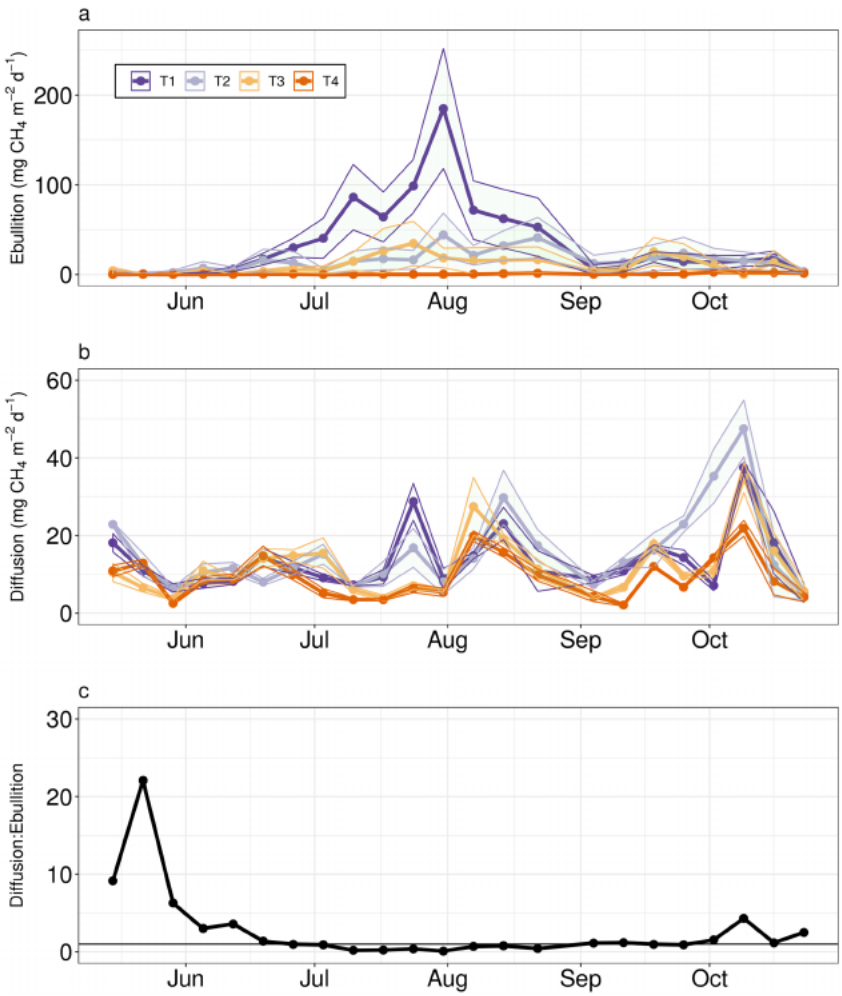

Figure 4. Mean daily transect CH_4 ebullition (a) and diffusion (b) rates observed during the 2017 ice-free monitoring period for transects T1–T4. The thin corresponding lines in (a) and (b) denote ±1 SE. The ratio of the mean daily diffusion to ebullition rate are shown for the whole reservoir in (c). The horizontal line in (c) represents the 1:1 diffusion: ebullition line.

We observed a shift in the reservoir-wide CH_{4diff}:CH_{4ebu} ratio during the monitoring period (Figure 4c). The reservoir-wide CH_{4diff}:CH_{4ebu} ratio was >1 from 15 May through 19 June before decreasing to <1 from 19 June through 22 August. During the week of 4 September, the CH_{4diff}:CH_{4ebu} ratio increased slightly to 1.3 and then decreased to <1 again from 11 to 25 September. During the period just before and after turnover (2–23 October), the CH_{4diff}:CH_{4ebu} ratio again increased to >1 as ebullition rates declined across all transects while diffusion rates increased (Figures 4a and 4b).

3.4. Spatial Changes in the Drivers of Ebullition and Diffusion

The spatiotemporal variability in CH_4 emissions in FCR was reflected in the variability of the potential environmental predictors measured at each transect (Figure 5). SWI temperatures exhibited expected seasonal trends, in which temperatures were low in the spring and increased into midsummer, peaking on 14 August, before decreasing into the fall (Figure 5a). SWI temperatures were warmest at T1 and T2 and 5.27–4.04°C lower at transects T3 and T4. The date of fall turnover in the reservoir was 17 October based on our criterion.

Unlike SWI temperature, near-sediment and surface water turbulence exhibited varying trends between FCR's transects (Figures 5b and 5c). The highest near-sediment turbulence occurred at T1 with a mean seasonal turbulence of 1.68 $e^{-6} \pm 8.13\ e^{-7}$ J kg^{-1}, compared to 1.22 $e^{-8} \pm 3.03\ e^{-9}$ J kg^{-1} at T4, which had the

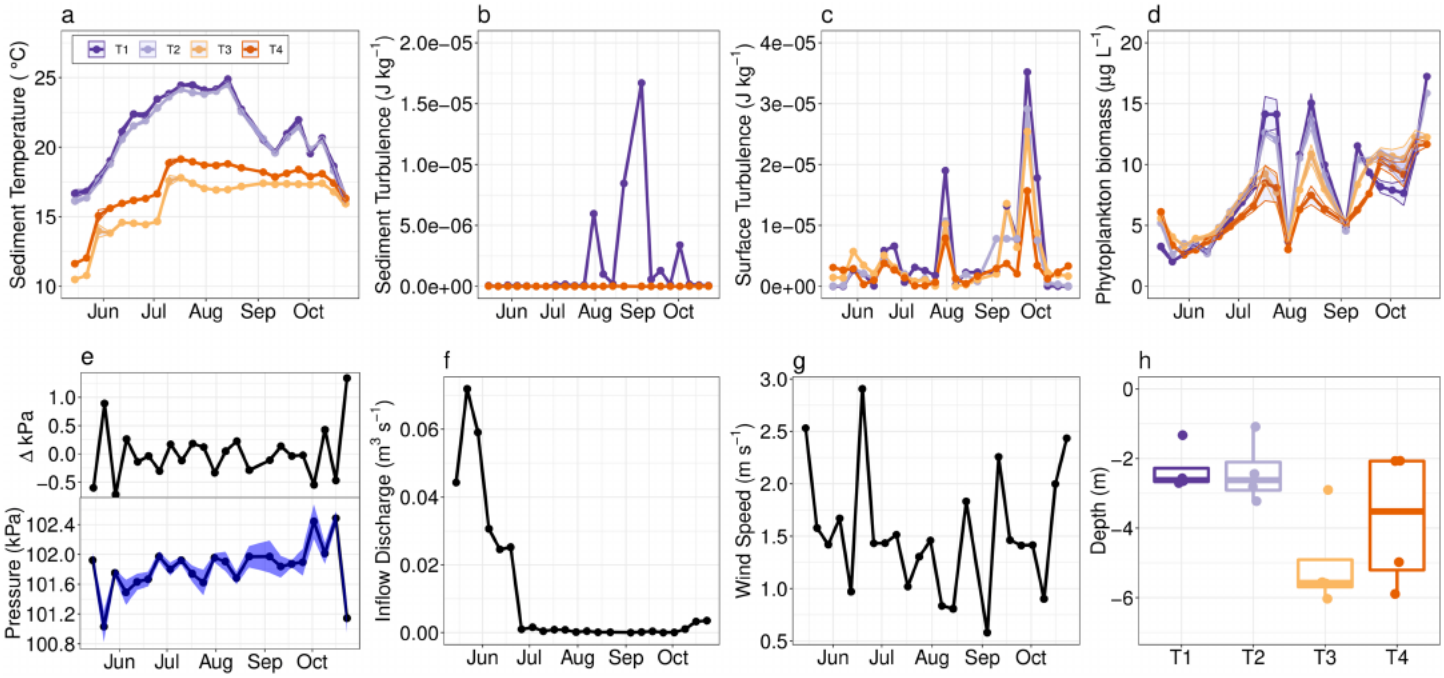

Figure 5. Time series of the eight predictor variables tested as drivers of ebullition and diffusion in FCR during the monitoring period (a–h) at transects T1–T4. These predictor variables included (a) mean weekly sediment-water interface temperatures averaged within each transect ±1 SE; mean weekly water turbulence at the (b) near-sediment and (c) water surface; (d) phytoplankton biomass ±1 SE; (e) the first difference of the mean week to week atmospheric pressure (a–d) with the mean weekly atmospheric pressure ± 1 SE shown for reference (e–h); (f) the mean weekly inflow discharge; (g) the mean wind speed during sampling days; and (h) the mean depth of each site within a transect.

lowest mean seasonal turbulence in the reservoir. The highest mean seasonal surface water turbulence occurred at T1 (5.46 e^{-6} ± 1.77 e^{-6} J kg^{-1}) and decreased downstream toward the dam, with the lowest surface turbulence at T4 (2.82 e^{-6} ± 6.85 e^{-7} J kg^{-1}).

The Δ *pressure* exhibited larger week-to-week changes both early and late in the monitoring period and remained relatively stable during the middle of the monitoring period (Figure 5e). In contrast, inflow discharge was greater than 0.02 m^3 s^{-1} from 15 May to 26 June and then substantially decreased to discharge less than 0.02 m^3 s^{-1} for the remainder of the sampling period (Figure 5f). Wind speed did not exhibit any directional trends during the monitoring period, and there were no weeks when the mean wind speed was greater than 3.0 m s^{-1} (Figure 5g).

Mean seasonal water column phytoplankton biomass was highest at transects T1 and T2 (8.0 ± 0.9 and 8.2 ± 0.8 µg L^{-1}, respectively) and lower at transects T3 and T4 (7.6 ± 0.6 and 6.5 ± 0.5 µg L^{-1}, respectively). Phytoplankton biomass exhibited fluctuations throughout the season (Figure 5d) and reached their highest biomass at the end of the summer monitoring season at all transects.

3.5. Environmental Drivers of CH_4 Emissions

3.5.1. Whole-Reservoir Emissions

Both physical and biological drivers were important predictors of ebullition and diffusion during the stratified period in FCR based on the AICc rankings. The best model for reservoir-wide seasonal ebullition rates showed a strong positive relationship with SWI temperature and wind speed and a negative relationship with inflow discharge (full model AICc = 44.0, $p < 0.0001$; Table 1). Reservoir-wide seasonal diffusion rates were best explained by a positive association with total phytoplankton biomass, but the relationship was much weaker (AICc = 33.2, $p = 0.05$; Table 1).

3.5.2. Transect-Specific Emissions

Physical factors were the most important drivers of ebullition in the best fitting models for transects T1–T3, while phytoplankton biomass was the most important driver of ebullition at transect T4 based on the models chosen by AICc (Table 1). At transect T1, ebullition rates were best predicted by a positive association with

Table 1
Time Series Models of CH_4 Ebullition and Diffusion Rates for the Aggregated Reservoir ("All," Shaded Rows) or the Individual Transects (T1–T4)

Efflux	Site	Time series model equation	Predictor(s)	AICc	p	R^2
Ebu	All	$\ln(ebu_t) = -5.11 \pm 1.14 + 0.37 \pm 0.09(AR1) + 0.30 \pm 0.08$ (SWI temp.) $+ 1.14 \pm 0.30$(wind speed) $- 0.53 \pm 0.25(\Delta$ *Press.*)	AR1 + SWI temp. + wind speed − Δ *Press.*	44.0	2.2×10^{-7}	0.86
Ebu	T1	$\ln(ebu_t) = -6.46 \pm 1.14 + 0.32 \pm 0.04(AR1) + 0.39 \pm 0.05$ (SWI temp.) $+ 0.39 \pm 0.05$(wind speed) $- 0.44 \pm 0.21(\Delta$ *Press.*)	AR1 + SWI temp. + wind speed − Δ *Press.*	38.6	4.8×10^{-12}	0.96
Ebu	T2	$\ln(ebu_t) = -2.36 \pm 0.96 + 0.04 \pm 0.11(AR1) + 0.16 \pm 0.05$ (SWI temp.) $- 0.20 \pm 0.07$(inflow)	AR1 + SWI temp. − inflow	46.8	1.1×10^{-5}	0.73
Ebu	T3	$\ln(ebu_t) = -2.18 \pm 1.20 - 0.29 \pm 0.23$ (AR1) $- 0.60 \pm 0.20$(inflow)	AR1 − inflow	95.0	0.02	0.34
Ebu	T4	$\ln(ebu_t) = -3.21 \pm 1.48 + 0.23 \pm 0.18$ (AR1) $+ 1.37 \pm 0.71$(phytoplankton)	AR1 + phytoplankton	81.2	0.009	0.37
Diff	All	$\ln(diff_t) = 1.11 \pm 0.56 + 0.26 \pm 0.20$ (AR1) $+ 0.38 \pm 0.19$(phytoplankton)	AR1 + phytoplankton	33.2	0.05	0.25
Diff	T1	$\ln(diff_t) = 2.49 \pm 0.59 - 0.01 \pm 0.22(AR1)$	AR1	39.0	0.97	0.01
Diff	T2	$\ln(diff_t) = 1.55 \pm 0.59 + 0.39 \pm 0.22(AR1)$	AR1	42.2	0.08	0.13
Diff	T3	$\ln(diff_t) = 1.71 \pm 0.51 + 0.25 \pm 0.22(AR1)$	AR1	47.2	0.26	0.06
Diff	T4	$\ln(diff_t) = 1.55 \pm 0.46 + 0.23 \pm 0.21(AR1)$	AR1	50.2	0.29	0.01

Note. Refer to Table S2 for all the models within less than two AICc units of the best fitting model shown and the null autoregressive (AR1) model for comparison. Additionally, refer to Table S1 for all of the models within less than two AICc units for each individual site in the reservoir, which were generally very similar to the aggregated transect-level results. SWI temperature is abbreviated as SWI temp. The weekly change in atmospheric pressure is represented by Δ *Press.*, and phytoplankton biomass is represented by phytoplankton. The weekly mean inflow discharge is represented by inflow.

SWI temperature and wind speed and a negative association with the *pressure* (AICc = 38.6, $p < 0.0001$; Table 1). Similar to T1, T2 ebullition rates were also best predicted by physical drivers, including a positive association with SWI temperature and a negative association with inflow discharge (AICc = 46.8, $p < 0.0001$; Table 1). The T3 transect was best predicted by a negative association with inflow (AICc = 95.0, $p = 0.02$). The best fitting model predicting ebullition rates at T4 changed from including physical variables to biological variables, with ebullition best predicted by a positive association with phytoplankton biomass (AICc = 81.2, $p = 0.009$).

The CH_4 diffusion models were much weaker than the CH_4 ebullition models. Across the reservoir, diffusion was best predicted by a positive association with phytoplankton biomass (AICc = 33.2, $p = 0.05$). For all individual transects, the best fitting model to predict diffusion was the AR1 lag term alone, with no environmental predictors (Table 1).

3.5.3. Assessment of Model Performance

The best fitting models for CH_4 ebullition rates were able to reproduce almost all of the dynamics in weekly CH_4 ebullition at the upstream transects in FCR (Table 1 and Figures 6a and 6e). Aggregated over the whole reservoir, the residuals from comparing the predicted versus observed ebullition were small throughout the monitoring period (Figure 6a). The predicted ebullition at T1 closely matched the observed patterns except for 31 July, when the model for the T1 transect slightly underestimated the observed rates (Figure 6b). The predicted ebullition at T2 also closely matched the observed patterns except for 31 July and 22 August, when the model also slightly underestimated the observed rates. At T3 and T4, the predicted ebullition rates were close to the observed rates at the end of the monitoring period but missed some variability in the early and midseason observations, resulting in weaker model fits (Table 1 and Figures 6d and 6e).

The best fitting models of CH_4 diffusion poorly predicted the weekly diffusion rates among transects but did slightly better at the whole-reservoir scale (Table 1 and Figures 6f and 6j). Aggregated to the whole reservoir, the residuals from comparing the predicted versus observed diffusion did not always capture large changes in the week-to-week variability and underestimated the peak diffusion rate that occurred during fall turnover. The predicted weekly diffusion rates at T1 were unable to capture any observed variability (Figure 6g). At T2 and T3, the best-predicted diffusion rates from both transects captured more week-to-week variability than at T1, but the model fits were poor, and predictions substantially underestimated diffusion rates at fall turnover (Figures 6h and 6i). Finally, the diffusion model for T4 was similar to T1 and was rarely able to capture the observed variability (Figure 6j).

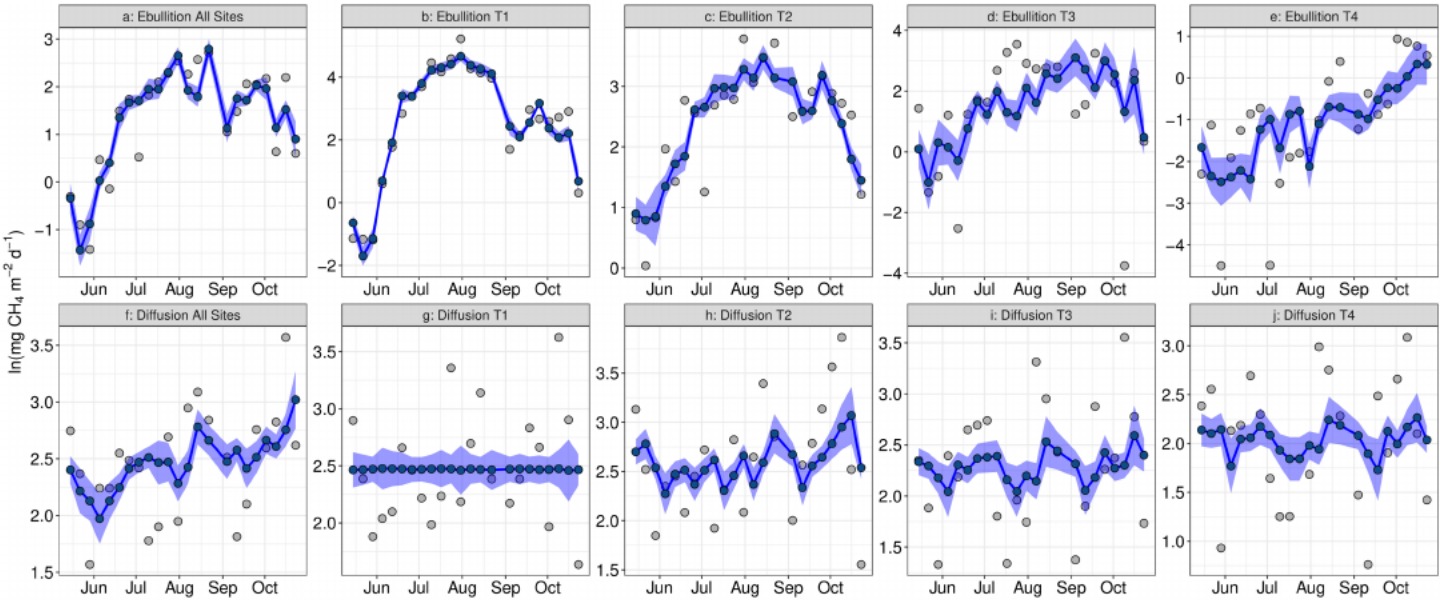

Figure 6. Time series of observed data (gray circles) and modeled ±1 SE (purple solid lines and shading) of CH_4 ebullition (a–e) and diffusion (f–j) aggregated across Falling Creek Reservoir (leftmost column) and at each transect along FCR's longitudinal gradient from 15 May through 23 October. The modeled data are from the best fitting AICc model for each CH_4 emission and transect (see Table 1). Note that the *y* axes of each row differ among plots.

4. Discussion

4.1. Drivers of CH_4 Ebullition Varied Spatially in a Small Reservoir

We observed substantial longitudinal variability in both the magnitude and the drivers of CH_4 ebullition in FCR, suggesting that the longitudinal heterogeneity in CH_4 emission rates that has been well documented in large reservoirs (e.g., DelSontro et al., 2010; Demarty et al., 2011; Marcelino et al., 2015) also exists in small reservoirs (<0.5 km^2). The varying importance of different drivers of ebullition along the longitudinal gradient in FCR suggests that multiple factors must be considered to predict reservoir-wide ebullition rates in smaller reservoirs. Our results underscore the need for improved spatial sampling of the rates and drivers of CH_4 ebullition in small reservoirs, which encompass the majority of documented reservoirs in the conterminous United States (National inventory of dams, 2018).

Ebullition was best predicted by physical variables at upstream transects T1–T3 and phytoplankton biomass at the downstream T4 transect during the monitoring period. The best fitting model for T1 ebullition exhibited positive associations with temperature and mean wind speed and a negative association with Δ *pressure*. Using FCR's longitudinal gradient as a guide, T1 is upstream of the primary inflow to FCR and below a wetland (Gerling et al., 2016), which likely had a strong influence on the CH_4 ebullition dynamics at this site. Wetlands are known to emit large quantities of CH_4via ebullition (reviewed in Whalen, 2005), and previous studies have found that the same physical variables in the best fitting model for T1 also drive ebullition rates in wetlands (Aben et al., 2017; Goodrich et al., 2011; Morin et al., 2014; Whalen, 2005). Additionally, the highest mean daily ebullition rate from T1 (185 mg CH_4 m^{-2} day^{-1}) is similar to rates observed in flooded wetland ecosystems (Whalen, 2005).

By comparison, ebullition at transects T2 and T3, which are just downstream of FCR's primary inflow, was driven by variables characteristic of riverine and transitional sites in larger reservoirs (Beaulieu et al., 2016). Ebullition rates at both T2 and T3 sites were driven by a negative association with inflow discharge, and ebullition at T2 also had a positive association with SWI temperature. Inflow discharge rate has been previously documented as an important driver of ebullition at locations in reservoirs where tributaries can deliver large quantities of organic matter that fuel methanogenesis and subsequent ebullition during periods of low discharge (Beaulieu et al., 2014, 2016, Maeck et al., 2014; Sobek et al., 2012; Wilkinson et al., 2015). When discharge is high, ebullition may be inhibited because of organic matter erosion and lower rates of

deposition at these sites (Beaulieu et al., 2016), thus resulting in the negative association between discharge and ebullition.

The most downstream transect (T4) was the only transect at which ebullition rates were driven by biological rather than physical drivers, suggesting that even along a short longitudinal gradient in a small reservoir, deeper downstream sites may have fundamentally different drivers of ebullition than shallower inflow sites. The significant positive association with phytoplankton biomass at T4 suggests that phytoplankton productivity at deeper, more lacustrine sites close to the dam may stimulate ebullition by providing labile autochthonous substrate to the sediments (West et al., 2016; Zhou et al., 2019). This finding is in contrast with upstream sites, which exhibited higher mean phytoplankton biomass, yet ebullition rates were still driven by physical factors such as inflow, wind speed, temperature, and pressure. These upstream sites displayed higher ebullition rates overall, suggesting that physical factors have the potential to be more important drivers of ebullition than biological factors in small reservoirs, as demonstrated by FCR's reservoir-wide ebullition model (Table 1).

Finally, it is important to note that there were alternate best fitting models for explaining ebullition rates that were within two AICc units of the top ebullition model for each transect. These alternate models included other physical variables and phytoplankton biomass (Table S2) but were in general very similar to the best fitting model reported in Table 1. However, depth was never included as a significant predictor in any of the best fitting AICc models. This may be because FCR is a relatively small and shallow reservoir ($Z_{max} = 9.3$ m), where ebullition was more likely related to the transect proximity to the inflow than changes in depth (DelSontro et al., 2011).

4.2. Reservoir-Wide CH_4 Diffusion Was Predicted by Phytoplankton

In contrast to ebullition, we could not identify unique drivers of diffusion among transects within FCR; rather, diffusion rates were best predicted at the whole-reservoir scale and were positively associated with phytoplankton biomass. Overall, the longitudinal variability in both the magnitude and drivers of CH_4 diffusion was much less than for ebullition. While CH_4 ebullition decreased by 98% from upstream T1 to downstream T4, diffusion only decreased by 32%. We also did not observe a shift in the importance of physical to biological predictors of CH_4 diffusion while moving toward the dam on the longitudinal gradient in FCR, as diffusion rates at all of the transects were not predicted by any of the measured environmental variables (Table 1). Despite not appearing in any of the site-specific models, phytoplankton biomass was the best predictor of diffusion at the whole-reservoir scale (Table 1). In the case of FCR, this result suggests that diffusion may be best predicted by a reservoir-wide analysis of drivers with observations from multiple sites.

Multiple mechanisms may explain why phytoplankton biomass was a significant predictor of the whole-reservoir diffusion rates. For example, senesced phytoplankton settling onto shallower sediments in both littoral and pelagic zones could increase methanogenesis (West et al., 2012), potentially stimulating diffusion rates from the sediments into the water column (Peeters et al., 2019). It is also possible that CH_4 production in oxic waters is affected by phytoplankton dynamics (Bižić et al., 2018; Bogard et al., 2014; Grossart et al., 2011; Yeung et al., 2017).

Surprisingly, wind speed was not a significant predictor of CH_4 diffusion at any transect or at the whole-reservoir scale, in contrast to earlier studies (Berg et al., 2017; Cole et al., 2010; Wanninkhof, 1992). However, FCR is a small, sheltered reservoir in a steep forested watershed that is protected from higher winds (Gerling et al., 2016). A similar spatiotemporal CH_4 emission study in naturally formed lakes also found that wind speed was not a significant predictor of CH_4 diffusion in two of the three lakes at the Skogaryd Research Catchment, Sweden (Natchimuthu et al., 2016). Following these conflicting results, we propose that wind speed may not be a substantial predictor of CH_4 diffusion in small, sheltered reservoirs but is likely still an important driver in lakes and reservoirs that are less wind sheltered.

4.3. Other Candidate Drivers and Caveats

There are also other possible drivers for both ebullition and diffusion that we did not measure in this study. For example, we were unable to measure transect-specific nutrient concentrations (e.g., nitrogen and phosphorus), which are known to be positively related to ebullition by stimulating phytoplankton growth (Davidson et al., 2018). We also did not quantitatively measure aquatic plant abundance, which has been

associated with CH_4 ebullition (Marinho et al., 2015) and diffusion (Attermeyer et al., 2016), though we note qualitatively that plant abundance at our transect sites was minimal. Diffusion was also likely underestimated because we assumed that diffusive rates were the same over a diel period when scaled from the short duration of time that we measured efflux. Thus, increases in CH_4 diffusion rates that occur during the night because of convective mixing (e.g., Anthony & MacIntyre, 2016; Deshmukh et al., 2014) were not accounted for in our study. Finally, we were also unable to measure sediment properties such as carbon quality (Zhou et al., 2019) and deposition rates, which can also influence CH_4 ebullition (Sobek et al., 2012; Wik et al., 2018).

It is also important to note that aggregating CH_4 emissions and environmental predictors to the week time scale may have masked the importance of turbulence and Δ *pressure* as significant drivers. For example, rapid decreases in barometric pressure and hydrostatic pressure that occur within short time periods (<24 hr) have been shown to substantially increase ebullition rates (Casper et al., 2000). Using alternate methods such as echo sounders (Ostrovsky, 2003; Tušer et al., 2017) and automated bubble traps (Delwiche & Hemond, 2017; Varadharajan et al., 2010) for measuring ebullition may provide insight on the drivers of ebullition rates at shorter time scales.

4.4. Variable Diffusion:Ebullition Ratios Over Both the Longitudinal Gradient and Time

Our data show that the dominant CH_4 emission pathway from the riverine zone was ebullition and the lacustrine zone was dominated by diffusion, resulting in diffusion:ebullition ratios less than one upstream and greater than one downstream. This pattern is primarily due to decreases in ebullition rates at downstream sites rather than increases in diffusion downstream. While ebullition is sometimes thought of as the dominant pathway of CH_4 emissions from reservoirs (e.g., DelSontro et al., 2010), our results follows other studies that observed ratios of diffusion to ebullition closer to one at the whole reservoir level (e.g., Barros et al., 2011; Deemer et al., 2016). Interestingly, many of these waterbodies with diffusion:ebullition ratios of ~1 are older reservoirs like FCR (Barros et al., 2011).

Our data also show that the CH_{4diff}:CH_{4ebu} ratio at the reservoir level can vary substantially throughout the ice-free period (Figure 4c), with spring and fall conditions dominated by diffusion and midsummer conditions dominated by ebullition. These findings follow studies from other northern latitude reservoirs in which elevated diffusion is observed in early spring immediately after ice-off (Huttunen et al., 2002), when ebullition is low. In midsummer, elevated ebullition is observed from the shallow riverine sites as the sediment temperatures warm (Aben et al., 2017), followed by elevated diffusion rates again in the late fall when thermal stratification weakens and deeper waters with high CH_4 concentrations mix to the surface. The shifts in the CH_{4diff}:CH_{4ebu} ratio observed throughout our 23-week monitoring period highlight the need for long-term monitoring efforts of both emissions at multiple sites in small reservoirs.

4.5. Lower CH_4 Emission Rates at FCR Relative to Other Reservoirs

FCR was a source of CH_4 to the atmosphere via both ebullition and diffusion, resulting in total emissions of 40.9 g CH_4 m^{-2} over the monitoring period. However, the overall magnitude of CH_4 emissions from FCR was low relative to ebullition and diffusion rates reported from other reservoirs. In comparison to 75 other reservoirs for which both ebullition and diffusion rates are available in a recent meta-analysis (Deemer et al., 2016), total CH_4 emissions from FCR were only ~30% of the mean CH_4 reservoir emissions. It is likely that FCR may have lower emission rates because our study was conducted ~120 years after FCR's construction, and older reservoirs such as FCR tend to have lower CH_4 emissions than younger reservoirs (Barros et al., 2011; Prairie et al., 2018).

5. Conclusions

While reservoir construction has slowed in some parts of the world, it has also increased dramatically in others (Zarfl et al., 2014), making reservoirs critical ecosystems to monitor for greenhouse gas emissions. By intensively sampling a small reservoir, we showed that CH_4 ebullition rates can substantially decrease along a longitudinal gradient while diffusion rates remain similar and that the dominant CH_4 emission type changed over the season. Our time series models reveal that multiple variables predict CH_4 ebullition along the longitudinal gradient of a small, shallow reservoir and that the relative importance of these drivers can

change substantially within a few hundred meters, while diffusion was better predicted by one variable at the whole-reservoir scale. The switch in the importance of drivers for ebullition rates along the longitudinal gradient in a small reservoir highlights the need to sample site-specific physical and biological drivers in conjunction with emission rates. As most reservoirs in the conterminous United States have a small surface area (National inventory of dams, 2018), estimating CH_4 emissions from these smaller waterbodies is critically important for informing upscaling of reservoir-specific estimates to the regional and global scale.

Author Contributions

R. P. M. and C. C. C. conceived the original research project, from which R. P. M., J. C. L., and C. C. C. worked closely together to develop the methods and ideas in this manuscript. R. P. M. led the overall analyses, data interpretation, and writing with C. C. C., R. P. M., M. E. L., and K. M. K. collected field data; S. C. calibrated and ran the 3-D hydrodynamic model; and R. P. M., M. E. L., S. C., and C. C. C. compiled and analyzed data. All authors approved the final version of the manuscript.

Acknowledgments
We thank the staff at the Western Virginia Water Authority for their long-term support and access to Falling Creek Reservoir, especially C. Brewer, J. Morris, G. Belcher, J. Booth, B. Benninger, and G. Robertson. We are eternally grateful to L. Finegold, M. Goodall, D. Howard, K. Farrell, N. Ward, J. Doubek, J. Famularo, T. McClure, N. McClure, and D. Swain for field help and L. Finegold and M. Goodall for data collation. B. Niederlehner, L. Finegold, M. Goodall, and D. Wiley provided crucial help and time analyzing samples. C. Lei and X. Man provided helpful feedback on the turbulence calculations. This work was financially supported by Grant 117105 from the Virginia Tech Graduate Research Development Program, the Virginia Tech Global Change Center, and National Science Foundation (NSF) Grants DEB-1753639, CNS-1737424, and EF-1702506. Supporting figures for the manuscript can be found in the supporting information. All data sets analyzed in this manuscript are cited therein and available in the Environmental Data Initiative (EDI) repository. The DOIs for the datasets are doi:10.6073/pasta/037384d2d5ae16cdc7450bf7a72792e3; doi:10.6073/pasta/64ff214b987da2997f5c823b156b3334; doi:10.6073/pasta/31691748ab0fa83430e6a65eeea29337; and doi:10.6073/pasta/8f6e3f85f1ec816d9f55cbbf060a507c.

References

Aben, R. C. H., Barros, N., van Donk, E., Frenken, T., Hilt, S., Kazanjian, G., et al. (2017). Cross continental increase in methane ebullition under climate change. *Nature Communications*, *8*(1), 1682. https://doi.org/10.1038/s41467-017-01535-y

Anthony, K. W., & MacIntyre, S. (2016). Nocturnal escape route for marsh gas. *Nature*, *535*(7612), 363–365. https://doi.org/10.1038/535363a

Attermeyer, K., Flury, S., Jayakumar, R., Fiener, P., Steger, K., Arya, V., et al. (2016). Invasive floating macrophytes reduce greenhouse gas emissions from a small tropical lake. *Scientific Reports*, *6*, 20424. https://doi.org/10.1038/srep20424

Barros, N., Huszar, V., Cole, J. J., Tranvik, L. J., Bastviken, D., del Giorgio, P. A., et al. (2011). Carbon emission from hydroelectric reservoirs linked to reservoir age and latitude. *Nature Geoscience*, *4*(9), 593–596. https://doi.org/10.1038/ngeo1211

Bastviken, D., Cole, J., Pace, M., & Tranvik, L. (2004). Methane emissions from lakes: Dependence of lake characteristics, two regional assessments, and a global estimate. *Global Biogeochemical Cycles*, *18*(4). https://doi.org/10.1029/2004GB002238

Beaulieu, J. J., Balz, D. A., Birchfield, M. K., Harrison, J. A., Nietch, C. T., Platz, M. C., et al. (2018). Effects of an experimental water-level drawdown on methane emissions from a eutrophic reservoir. *Ecosystems*, *21*(4), 657–674. https://doi.org/10.1007/s10021-017-0176-2

Beaulieu, J. J., McManus, M. G., & Nietch, C. T. (2016). Estimates of reservoir methane emissions based on a spatially balanced probabilistic-survey. *Limnology and Oceanography*, *61*(S1), S27–S40. https://doi.org/10.1002/lno.10284

Beaulieu, J. J., Smolenski, R. L., Nietch, C. T., Townsend-Small, A., & Elovitz, M. S. (2014). High methane emissions from a midlatitude reservoir draining an agricultural watershed. *Environmental Science & Technology*, *48*(19), 11,100–11,108. https://doi.org/10.1021/es501871g

Bižić, M., Klintzsch, T., Ionescu, D., Hindiyeh, M. Y., Günthel, M., Muro-Pastor, A. M. ... et al. (2020). Aquatic and terrestrial cyanobacteria produce methane. *Science Advances*, *6*(3), eaax5343. https://doi.org/10.1126/sciadv.aax5343

Bogard, M. J., del Giorgio, P. A., Boutet, L., Chaves, M. C. G., Prairie, Y. T., Merante, A., & Derry, A. M. (2014). Oxic water column methanogenesis as a major component of aquatic CH_4 fluxes. *Nature Communications*, *5*, 5350. https://doi.org/10.1038/ncomms6350

Box, G. E., & Pierce, D. A. (1970). Distribution of residual autocorrelations in autoregressive-integrated moving average time series models. *Journal of the American Statistical Association*, *65*(332), 1509–1526. https://www.jstor.org/stable/2284333

Carey, C. C., Bookout, B. J., Lofton, M. E., & McClure, R. P. (2019). Time series of high-frequency meteorological data at Falling Creek Reservoir, Virginia, USA 2015-2018. *Environmental Data Initiative.*. https://doi.org/10.6073/pasta/037384d2d5ae16cdc7450bf7a72792e3

Carey, C. C., Gerling, A. B., McClure, R. P., Lofton, M. E., & Bookout, B. J. (2018). Discharge time series for the primary inflow tributary entering Falling Creek Reservoir, Vinton, Virginia, USA 2013-2018. *Environmental Data Initiative.*. https://doi.org/10.6073/pasta/64ff214b987da2997f5c823b156b3334

Carey, C. C., Lofton, M. E., Hamre, K. D., Doubek, J. P., & McClure, R. P. (2018). Time-series of high-frequency profiles of fluorescence-based phytoplankton spectral groups in Beaverdam Reservoir, Carvins Cove Reservoir, Falling Creek Reservoir, Gatewood Reservoir, and Spring Hollow Reservoir in southwestern Virginia, USA 2013-2017. *Environmental Data Initiative.*. https://doi.org/10.6073/pasta/31691748ab0fa83430e6a65eeea29337

Carey, C. C., Weathers, K. C., Ewing, H. A., Greer, M. L., & Cottingham, K. L. (2014). Spatial and temporal variability in recruitment of the cyanobacterium Gloeotrichia echinulata in an oligotrophic lake. *Freshwater Science*, *33*(2), 577–592. https://doi.org/10.1086/675734

Casper, P., Maberly, S. C., Hall, G. H., & Finlay, B. J. (2000). Fluxes of methane and carbon dioxide from a small productive lake to the atmosphere. *Biogeochemistry*, *49*(1), 1–19. https://doi.org/10.1023/A:1006269900174

Catherine, A., Escoffier, N., Belhocine, A., Nasri, A. B., Hamlaoui, S., Yéprémian, C., et al. (2012). On the use of the FluoroProbe®, a phytoplankton quantification method based on fluorescence excitation spectra for large-scale surveys of lakes and reservoirs. *Water Research*, *46*(6), 1771–1784. https://doi.org/10.1016/J.WATRES.2011.12.056

Chen, S., Carey, C. C., Little, J. C., Lofton, M. E., McClure, R. P., & Lei, C. (2018). Effectiveness of a bubble-plume mixing system for managing phytoplankton in lakes and reservoirs. *Ecological Engineering*, *113*, 43–51. https://doi.org/10.1016/j.ecoleng.2018.01.002

Chen, S., Lei, C., Carey, C. C., Gantzer, P. A., & Little, J. C. (2017). A coupled three-dimensional hydrodynamic model for predicting hypolimnetic oxygenation and epilimnetic mixing in a shallow eutrophic reservoir. *Water Resources Research*, *53*(1), 470–484. https://doi.org/10.1002/2016WR019279

Cole, J. J., Bade, D. L., Bastviken, D., Pace, M. L., & Van de Bogert, M. (2010). Multiple approaches to estimating air-water gas exchange in small lakes. *Limnology and Oceanography: Methods*, *8*(6), 285–293. https://doi.org/10.4319/lom.2010.8.285

Davidson, T. A., Audet, J., Jeppesen, E., Landkildehus, F., Lauridsen, T. L., Søndergaard, M., & Syväranta, J. (2018). Synergy between nutrients and warming enhances methane ebullition from experimental lakes. *Nature Climate Change*, *8*(2), 156–160. https://doi.org/10.1038/s41558-017-0063-z

Deemer, B. R., Harrison, J. A., Li, S., Beaulieu, J. J., DelSontro, T., Barros, N., et al. (2016). Greenhouse gas emissions from reservoir water surfaces: A new global synthesis. *Bioscience*, *66*(11), 949–964. https://doi.org/10.1093/biosci/biw117

DelSontro, T., Beaulieu, J. J., & Downing, J. A. (2018). Greenhouse gas emissions from lakes and impoundments: Upscaling in the face of global change. *Limnology and Oceanography Letters*, *3*(3), 64–75. https://doi.org/10.1002/lol2.10073

DelSontro, T., Boutet, L., St-Pierre, A., del Giorgio, P. A., & Prairie, Y. T. (2016). Methane ebullition and diffusion from northern ponds and lakes regulated by the interaction between temperature and system productivity. *Limnology and Oceanography*, *61*(S1), S62–S77. https://doi.org/10.1002/lno.10335

DelSontro, T., Kunz, M. J., Kempter, T., Wüest, A., Wehrli, B., & Senn, D. B. (2011). Spatial heterogeneity of methane ebullition in a large tropical reservoir. *Environmental Science & Technology*, *45*(23), 9866–9873. https://doi.org/10.1021/es2005545

DelSontro, T., Mcginnis, D. F., Sobek, S., Ostrovsky, I., & Wehrli, B. (2010). Extreme methane emissions from a swiss hydropower reservoir: Contribution from bubbling sediments. *Environmental Science & Technology*, *44*(7), 2419–2425. https://doi.org/10.1021/es9031369

Delwiche, K., & Hemond, H. F. (2017). An enhanced bubble size sensor for long-term ebullition studies. *Limnology and Oceanography: Methods*, *15*(10), 821–835. https://doi.org/10.1002/lom3.10201

Demarty, M., Bastien, J., & Tremblay, A. (2011). Annual follow-up of gross diffusive carbon dioxide and methane emissions from a boreal reservoir and two nearby lakes in Québec, Canada. *Biogeosciences*, *8*(1), 41–53. https://doi.org/10.5194/bg-8-41-2011

Deshmukh, C., Serça, D., Delon, C., Tardif, R., Demarty, M., Jarnot, C., et al. (2014). Physical controls on CH_4 emissions from a newly flooded subtropical freshwater hydroelectric reservoir: Nam Theun 2. *Biogeosciences*, *11*(15), 4251–4269. https://doi.org/10.5194/bg-11-4251-2014

Gålfalk, M., Bastviken, D., Fredriksson, S., & Arneborg, L. (2013). Determination of the piston velocity for water-air interfaces using flux chambers, acoustic Doppler velocimetry, and IR imaging of the water surface. *Journal of Geophysical Research – Biogeosciences*, *118*(2), 770–782. https://doi.org/10.1002/jgrg.20064

Garratt, J. R. (1994). The atmospheric boundary layer. *Earth Science Reviews*, *37*(1-2), 89-134. https://doi.org/10.1016/0012-8252(94)90026-4

Gerling, A. B., Munger, Z. W., Doubek, J. P., Hamre, K. D., Gantzer, P. A., Little, J. C., & Carey, C. C. (2016). Whole-catchment manipulations of internal and external loading reveal the sensitivity of a century-old reservoir to hypoxia. *Ecosystems*, *19*(3), 555–571. https://doi.org/10.1007/s10021-015-9951-0

Grossart, H. P., Frindte, K., Dziallas, C., Eckert, W., & Tang, K. W. (2011). Microbial methane production in oxygenated water column of an oligotrophic lake. *Proceedings of the National Academy of Sciences*, *108*(49), 19657–19661. https://doi.org/10.1073/pnas.1110716108

Gunkel, G. (2009). Hydropower—A green energy? Tropical reservoirs and greenhouse gas emissions. *Clean: Soil, Air, Water*, *37*(9), 726–734. https://doi.org/10.1002/clen.200900062

Hofmann, H. (2013). Spatiotemporal distribution patterns of dissolved methane in lakes: How accurate are the current estimations of the diffusive flux path? *Geophysical Research Letters*, *40*(11), 2779–2784. https://doi.org/10.1002/grl.50453

Huang, Y., Yasarer, L. M. W., Li, Z., Sturm, B. S. M., Zhang, Z., Guo, J., & Shen, Y. (2017). Air–water CO_2 and CH_4 fluxes along a river–reservoir continuum: Case study in the Pengxi River, a tributary of the Yangtze River in the Three Gorges Reservoir, China. *Environmental Monitoring and Assessment*, *189*(5), 223. https://doi.org/10.1007/s10661-017-5926-2

Huttunen, J. T., Väisänen, T. S., Hellsten, S. K., Heikkinen, M., Nykänen, H., Jungner, H., et al. (2002). Fluxes of CH_4, CO_2, and N_2O in hydroelectric reservoirs Lokka and Porttipahta in the northern boreal zone in Finland. *Global Biogeochemical Cycles*, *16*(1), 3–1. https://doi.org/10.1029/2000GB001316

Joyce, J., & Jewell, P. W. (2003). Physical controls on methane ebullition from reservoirs and lakes. *Environmental and Engineering Geoscience*, *9*(2), 167–178. https://doi.org/10.2113/9.2.167

Keller, M., & Stallard, R. F. (1994). Methane emission by bubbling from Gatun Lake, Panama. *Journal Geophysical Research*, *99*(D4), 8307–8319. https://doi.org/10.1029/92JD02170

Kring, S. A., Figary, S. E., Boyer, G. L., Watson, S. B., & Twiss, M. R. (2014). Rapid in situ measures of phytoplankton communities using the bbe FluoroProbe: Evaluation of spectral calibration, instrument intercompatibility, and performance range. *Canadian Journal of Fisheries and Aquatic Sciences*, *71*(7), 1087–1095. https://doi.org/10.1139/cjfas-2013-0599

Maeck, A., DelSontro, T., McGinnis, D. F., Fischer, H., Flury, S., Schmidt, M., Fietzek, P., &Lorke, A. (2014). Sediment trapping by dams creates methane emission hot spots. *Environmental Science & Technology*, *47*(15), 8130–8137. https://doi.org/10.1021/es4003907

Marcelino, A. A., Santos, M. A., Xavier, V. L., Bezerra, C. S., Silva, C. R. O., Amorim, M. A., & Rogerio, J. P. (2015). Diffusive emission of methane and carbon dioxide from two hydropower reservoirs in Brazil. *Brazilian Journal of Biology*, *75*(2), 331–338. https://doi.org/10.1590/1519-6984.12313

Marinho, C. C., Palma-Silva, C., Albertoni, E. F., Giacomini, I. B., Barros, M. P. F., Furlanetto, L. M., & Esteves, F. de A. (2015). Emergent macrophytes alter the sediment composition in a small, shallow subtropical lake: Implications for methane emission. *American Journal of Plant Sciences*, *6*(02), 315–322. https://doi.org/10.4236/ajps.2015.62036

Martinez, D., & Anderson, M. A. (2013). Methane production and ebullition in a shallow, artificially aerated, eutrophic temperate lake (Lake Elsinore, CA). *Science Total Environment*, *454-455*, 457–465. https://doi.org/10.1016/j.scitotenv.2013.03.040

Mattson, M. D., & Likens, G. E. (1990). Air pressure and methane fluxes. *Nature*, *347*(6295), 718. https://doi.org/10.1038/347718b0

McClure, R. P., Hamre, K. D., Niederlehner, B. R., Munger, Z. W., Chen, S., Lofton, M. E., et al. (2018). Metalimnetic oxygen minima alter the vertical profiles of carbon dioxide and methane in a managed freshwater reservoir. *Science Total Environment*, *636*, 610–620. https://doi.org/10.1016/j.scitotenv.2018.04.255

McClure, R. P., Lofton, M. E., Chen, S., Krueger, K. M., Little, J. C., & Carey, C. C. (2019). Methane ebullition and diffusion rates, turbulence, water temperature, and water depth data from Falling Creek Reservoir in the ice-free period of 2017. *Environmental Data Initiative*.. https://doi.org/10.6073/pasta/8f6e3f85f1ec816d9f55cbbf060a507c

Morin, T. H., Bohrer, G., Frasson, R. D. M., Naor-Azreli, L., Mesi, S., Stefanik, K. C., & Schäfer, K. V. R. (2014). Environmental drivers of methane fluxes from an urban temperate wetland park. *Journal of Geophysical Research. Biogeosciences*, *119*(11), 2188–2208. https://doi.org/10.1002/2014JG002750

Myhre, G., Shindell, D., Bréon, F.-M., Collins, W., Fuglestvedt, J., Huang, J., et al. (2013). Anthropogenic and natural radiative forcing. Climate Change 2013: The Physical Science Basis. *Contribution of Working Group I to the Fifth Assessment Report of the Intergovernmental Panel on Climate Change*, *423*, 659–740. https://doi.org/10.1017/CBO9781107415324.018

Natchimuthu, S., Sundgren, I., Gålfalk, M., Klemedtsson, L., Crill, P., Danielsson, Å., & Bastviken, D. (2016). Spatio-temporal variability of lake CH_4 fluxes and its influence on annual whole lake emission estimates. *Limnology and Oceanography*, *61*(S1), S13–S26. https://doi.org/10.1002/lno.10222

National inventory of dams 2018. Washington, DC: US Army Corps of Engineers: Federal Emergency Management Agency. https://nid.sec.usace.army.mil, .

Ostrovsky, I. (2003). Methane bubbles in Lake Kinneret: Quantification and temporal and spatial heterogeneity. *Limnology and Oceanography*, *48*(3), 1030–1036. https://doi.org/10.4319/lo.2003.48.3.1030

Ouellet Jobin, V., & Beisner, B. E. (2014). Deep chlorophyll maxima, spatial overlap and diversity in phytoplankton exposed to experimentally altered thermal stratification. *Journal of Plankton Research*, *36*(4), 933–942. https://doi.org/10.1093/plankt/fbu036

Peeters, F., Encinas Fernandez, J., & Hofmann, H. (2019). Sediment fluxes rather than oxic methanogenesis explain diffusive CH_4 emissions from lakes and reservoirs. *Scientific Reports*, *9*(1), 1–10. https://doi.org/10.1038/s41598-018-36530-w

Peltola, O., Raivonen, M., Li, X., & Vesala, T. (2018). Technical note: Comparison of methane ebullition modelling approaches used in terrestrial wetland models. *Biogeosciences*, *15*, 937–951. https://doi.org/10.5194/bg-15-937-2018

Podgrajsek, E., Sahlée, E., Bastviken, D., Holst, J., Lindroth, A., Tranvik, L., & Rutgersson, A. (2014). Comparison of floating chamber and eddy covariance measurements of lake greenhouse gas fluxes. *Biogeosciences*, *11*(15), 4225–4233. https://doi.org/10.5194/bg-11-4225-2014

Poindexter, C. M., Baldocchi, D. D., Matthes, J. H., Knox, S. H., & Variano, E. A. (2016). The contribution of an overlooked transport process to a wetland's methane emissions. *Geophysical Research Letters*, *43*(12), 6276–6284. https://doi.org/10.1002/2016GL068782

Poindexter, C. M., & Variano, E. A. (2013). Gas exchange in wetlands with emergent vegetation: The effects of wind and thermal convection at the air-water interface. *Journal of Geophysical Research – Biogeosciences*, *118*(3), 1297–1306. https://doi.org/10.1002/jgrg.20099

Prairie, Y. T., Alm, J., Beaulieu, J., Barros, N., Battin, T., Cole, J., et al. (2018). Greenhouse gas emissions from freshwater reservoirs: What does the atmosphere see? *Ecosystems*, 1–14. https://doi.org/10.1007/s10021-017-0198-9

Quinn, G., & Keough, M. (2002). *Experimental design and data analysis for biologists*. Cambridge: Cambridge University Press. https://doi.org/10.1017/CBO9780511806384

R Core Team (2018). R: A language and environment for statistical computing. R Foundation for Statistical Computing, Vienna, Austria. URL https://www.R-project.org/.

Rueda, F., & Schladow, G. (2009). Mixing and stratification in lakes of varying horizontal length scales: Scaling arguments and energy partitioning. *Limnology and Oceanography*, *54*(6), 2003–2017. https://doi.org/10.4319/lo.2009.54.6.2003

Rueda, F. J., & Schladow, S. G. (2003). Dynamics of large polymictic lake. II: Numerical simulations. *Journal of Hydraulic Engineering*, *129*(2), 92-101. https://doi.org/10.4319/lo.2009.54.6.2003 (ASCE)0733-9429(2003)129:2(92)

Saunois, M., Bousquet, P., Poulter, B., Peregon, A., Ciais, P., Canadell, J. G., et al. (2016). The global methane budget 2000–2012. *Earth System Science Data*, *8*(2), 697–751. https://doi.org/10.5194/essd-8-697-2016

Schwarz, J. I. K., Eckert, W., & Conrad, R. (2008). Response of the methanogenic microbial community of a profundal lake sediment (Lake Kinneret, Israel) to algal deposition. *Limnology and Oceanography*, *53*(1), 113–121. https://doi.org/10.4319/lo.2008.53.1.0113

Smith, P. E. (2006). A semi-implicit, three-dimensional model for estuarine circulation in cooperation with the interagency ecological program for the San Francisco bay-delta estuary. USGS report No. 2006-1004. https://pubs.usgs.gov/of/2006/1004/pdf/ofr2006-1004.pdf

Sobek, S., DelSontro, T., Wongfun, N., & Wehrli, B. (2012). Extreme organic carbon burial fuels intense methane bubbling in a temperate reservoir. *Geophysical Research Letters*, *39*(1). https://doi.org/10.1029/2011GL050144

Soumis, N., Duchemin, É., Canuel, R., & Lucotte, M. (2004). Greenhouse gas emissions from reservoirs of the western United States. *Global Biogeochemical Cycles*, 18(3). https://doi.org/10.1029/2003GB002197

Tokida, T., Miyazaki, T., & Mizoguchi, M. (2005). Ebullition of methane from peat with falling atmospheric pressure. *Geophysical Research Letters*, *32*(13). https://doi.org/10.1029/2005GL022949

Tokida, T., Miyazaki, T., Mizoguchi, M., Nagata, O., Takakai, F., Kagemoto, A., & Hatano, R. (2007). Falling atmospheric pressure as a trigger for methane ebullition from peatland. *Global Biogeochemical Cycles*, *21*(2). https://doi.org/10.1029/2006GB002790

Tušer, M., Picek, T., Sajdlová, Z., Jůza, T., Muška, M., & Frouzová, J. (2017). Seasonal and spatial dynamics of gas ebullition in a temperate water-storage reservoir. *Water Resources Research*, *53*(10), 8266–8276. https://doi.org/10.1002/2017WR020694

Varadharajan, C., Hermosillo, R., & Hemond, H. F. (2010). A low-cost automated trap to measure bubbling gas fluxes. *Limnology and Oceanography: Methods*, *8*(7), 363–375. https://doi.org/10.4319/lom.2010.8.363

Wanninkhof, R. (1992). Relationship between wind speed and gas exchange. *Journal of Geophysical Research, Oceans*, *97*(92), 7373–7382. https://doi.org/10.1029/92JC00188

West, W. E., Coloso, J. J., & Jones, S. E. (2012). Effects of algal and terrestrial carbon on methane production rates and methanogen community structure in a temperate lake sediment. *Freshwater Biology*, *57*(5), 949–955. https://doi.org/10.1111/j.1365-2427.2012.02755.x

West, W. E., Creamer, K. P., & Jones, S. E. (2016). Productivity and depth regulate lake contributions to atmospheric methane. *Limnology and Oceanography*, *61*(S1), S51–S61. https://doi.org/10.1002/lno.10247

Whalen, S. C. (2005). Biogeochemistry of methane exchange between natural wetlands and the atmosphere. *Environmental Engineering Science*, *22*(1), 73–94. https://doi.org/10.1089/ees.2005.22.73

Wik, M., Johnson, J. E., Crill, P. M., DeStasio, J. P., Erickson, L., Halloran, M. J., et al. (2018). Sediment characteristics and methane ebullition in three subarctic lakes. *Journal of Geophysical Research – Biogeosciences*, *123*(8), 2399–2411. https://doi.org/10.1029/2017JG004298

Wik, M., Thornton, B. F., Bastviken, D., Uhlbäck, J., & Crill, P. M. (2016). Biased sampling of methane release from northern lakes: A problem for extrapolation. *Geophysical Research Letters*, *43*(3), 1256–1262. https://doi.org/10.1002/2015GL066501

Wilkinson, J., Maeck, A., Alshboul, Z., & Lorke, A. (2015). Continuous seasonal river ebullition measurements linked to sediment methane formation. *Environmental Science & Technology*, *49*(22), 13121–13129. https://doi.org/10.1021/acs.est.5b01525

Yang, L., Lu, F., Wang, X., Duan, X., Song, W., Sun, B., et al. (2013). Spatial and seasonal variability of diffusive methane emissions from the Three Gorges Reservoir. *Journal of Geophysical Research – Biogeosciences*, *118*(2), 471–481. https://doi.org/10.1002/jgrg.20049

Yeung, T., Kwan, M., Adler, L., Mills, T. J., Neilan, B. A., Conibeer, G., & Patterson, R. (2017). Increased methane production in cyanobacteria and methanogenic microbe co-cultures. *Bioresource Technology*, *243*, 686–692. https://doi.org/10.1016/j.biortech.2017.06.126

Yu, Z., Slater, L. D., Schäfer, K. V. R., Reeve, A. S., & Varner, R. K. (2014). Dynamics of methane ebullition from a peat monolith revealed from a dynamic flux chamber system. *Journal of Geophysical Research – Biogeosciences*, *119*(9), 1789–1806. https://doi.org/10.1002/2014JG002654

Zarfl, C., Lumsdon, A. E., Berlekamp, J., Tydecks, L., & Tockner, K. (2014). A global boom in hydropower dam construction. *Aquatic Sciences*, *77*(1), 161–170. https://doi.org/10.1007/s00027-014-0377-0

Zhou, Y., Zhou, L., Zhang, Y., de Souza, J. G., Podgorski, D. C., Spencer, R. G., et al. (2019). Autochthonous dissolved organic matter potentially fuels methane ebullition from experimental lakes. *Water Research*, 115048. https://doi.org/10.1016/j.watres.2019.115048

Zhu, D., Wu, Y., Chen, H., He, Y., & Wu, N. (2016). Intense methane ebullition from open water area of a shallow peatland lake on the eastern Tibetan Plateau. *Science Total Environment*, *542*, 57–64. https://doi.org/10.1016/j.scitotenv.2015.10.087